Freely Dispersible Au@TiO2, Au@ZrO2, Ag@TiO2, and Ag@ZrO2 CoreâShell Nanoparticles: One−Step Synthesis, Characterization, Spectroscopy, and Optical Limiting Properties

ARTICLE *in* LANGMUIR · APRIL 2003

Impact Factor: 4.46 · DOI: 10.1021/la0266435

Freely Dispersible $Au@TiO_2$, $Au@ZrO_2$, $Ag@TiO_2$, and $Ag@ZrO_2$ Core−Shell Nanoparticles: One-Step Synthesis, Characterization, Spectroscopy, and Optical Limiting Properties

Renjis T. Tom,[†] A. Sreekumaran Nair,[†] Navinder Singh,[‡] M. Aslam,[§] C. L. Nagendra,[||] Reji Philip,*[,‡] K. Vijayamohanan,*[,§] and T. Pradeep*[,†]

Department of Chemistry and Regional Sophisticated Instrumentation Centre, Indian Institute of Technology Madras, Chennai 600 036, India, Optics Group, Raman Research Institute, Bangalore 560 080, India, Physical and Materials Chemistry Division, National Chemical Laboratory, Dr. Homi Bhabha Road, Pune 411 008, India, and Laboratory for Electro-Optics Systems, A6 Peenya Industrial Estate, Bangalore 560 058, India

Received October 2, 2002. In Final Form: January 18, 2003

We report a one-step route for the synthesis of $Au@TiO_2$, $Au@ZrO_2$, $Ag@TiO_2$, and $Ag@ZrO_2$ particles in nanometer dimensions, with controllable shell thickness. This scalable procedure leads to stable and freely dispersible particles, and bulk nanocomposite materials have been made this way. The procedure leads to particles of various morphologies, with a crystalline core in the size range of 30−60 nm diameter and an amorphous shell of ∼3 nm thickness in a typical synthesis. The core diameter and shell thickness (in the range of 1−10 nm) can be varied, leading to different absorption maxima. The material has been characterized with microscopic, diffraction, and spectroscopic techniques. The metal particle growth occurs by the carbamic acid reduction route followed by hydrolysis of the metal oxide precursor, resulting in the oxide cover. The particles could be precipitated and redispersed. The shell, upon thermal treatment, gets converted to crystalline oxides. Cyclic voltammetric studies confirm the core−shell structure. The $E_{1/2}$ value is 0.250 V ($\Delta E \approx 180$ mV) for the quasi-reversible Ag_m/Ag_m^+ couple and 0.320 V ($\Delta E \approx 100$ mV) for the Au_n/Au_n^+ couple for Ag and Au particles, respectively. Adsorption on the oxide surface blocks electron transfer partially. Nonlinear optical measurements in solutions show that these materials are strong optical limiters with a high laser damage threshold.

Introduction

Core−shell metal nanoparticles is an emerging and active area of contemporary science.[1] While most of the research in this area has been on noble-metal nanocores and molecular shells, there has been a slow and steady growth of activity on nanomaterials with chalcogenide shells.[2−5] Monolayers anchored onto metal cores have been used as precursors to make oxide shells.[6,7] An approach in this direction has been used to make silica-coated gold clusters.[7] We have used a similar method in the synthesis of ZrO_2-covered nanoparticles of silver.[8] In all these methodologies, the monolayer cover is important, as the chemistry is specific to the shell. The monolayer route to oxide-shell materials is rather involved and requires multistep processes, and scale-up is difficult. It is in this context that we decided to explore the possibility of a one-step method using the well-known reduction of noble metals with dimethylformamide (DMF) in the presence of oxide-forming precursors used by Liz-Marzan et al. for the synthesis of $Ag@TiO_2$.[5] In this paper, we focus on the synthesis and characterization of TiO_2- and ZrO_2-covered Au and Ag redissolvable particles.

We initiated the work on oxide-protected metal colloids because this is one way to make metal nanoparticles stable under extreme conditions. Our recent work on optical nonlinearity has shown that these materials are some of the best optical limiters known thus far.[9] However, at high light intensities, they are susceptible to damage, leading to photofragmentation,[10] ligand desorption, etc. To make them stable at extreme conditions, it is necessary to protect them with stable and chemically inert shells such as oxides. As will be discussed below, we irradiated these oxide-protected colloids with laser pulses of intensities up to 2.8 GW/cm^2, and no sign of laser-induced damage was observed. This kind of cover also makes it possible to fabricate/process materials in the form of thin films and disks for applications. Initial results in these directions

* To whom correspondence should be addressed. E-mail: pradeep@iitm.ac.in (T.P.), viji@ems.ncl.res.in (K.V.), reji@rri.res.in (R.P.). Fax: 00-91-44-2257-0509 (0545) (T.P.).

[†] Indian Institute of Technology Madras.

[‡] Raman Research Institute.

[§] National Chemical Laboratory.

[||] Laboratory for Electro-Optics Systems.

(1) Zhong, C.-J.; Maye, M. M. *Adv. Mater.* **2001**, *13*, 1507−1511.

(2) Dabbousi, B. O.; Rodriguez-Viejo, J.; Mikulec, F. V.; Heine, J. R.; Mattoussi, H.; Ober, R.; Jensen, K. F.; Bawendi, M. G. *J. Phys. Chem. B* **1997**, *101*, 9463−9475.

(3) Danek, P.-S. M.; Jensen, K. F.; Murray, C. B.; Bawendi, M. G. *Chem. Mater.* **1996**, *8*, 173−180.

(4) Peng, X. G.; Schlamp, M. C.; Kadavanich, A. V.; Alivisatos, A. P. *J. Am. Chem. Soc.* **1997**, *119*, 7019−7029.

(5) (a) Pastoriza-Santos, I.; Liz-Marzan, L. M. *Langmuir* **1999**, *15*, 948−951. (b) Pastoriza-Santos, I.; Koktysh, D. S.; Mamedov, A. A.; Giersig. M.; Kotov, N. A.; Liz-Marzan, L. M. *Langmuir* **2000**, *16*, 2731−2735.

(6) Ung, T.; Liz-Marzan. L. M.; Mulvaney, P. *J. Phys. Chem. B* **1999**, *103*, 6770−6773.

(7) Liz-Marzan, L. M.; Giersig, M.; Mulvaney, P. *Langmuir* **1996**, *12*, 4329−4335.

(8) Eswaranand, V.; Pradeep, T. *J. Mater. Chem.* **2002**, *12*, 2421−2425.

(9) Philip, R.; Ravindra Kumar, R.; Sandhyarani, N.; Pradeep, T. *Phys. Rev. B* **2000**, *62*, 13160−13166.

(10) (a) Sun, Y. P.; Riggs, J. E.; Rollins, H. W.; Guduru, R. *J. Phys. Chem. B* **1999**, *103*, 77. (b) Kamat, P. V.; Flumiani, M.; Hartland, G. V. *J. Phys. Chem. B* **1998**, *102*, 3123. (c) Link, S.; Burda, D.; Nikoobakht, B.; El-Sayed, M. A. *J. Phys. Chem. B* **2000**, *104*, 6152. (d) Fujiwara, H.; Yanagida, S.; Kamat, P. V. *J. Phys. Chem. B* **1999**, *103*, 2589.

10.1021/la0266435 CCC: $25.00
Published on Web 03/07/2003

have been very promising and will constitute the subject matter of another publication.

Particles with oxide shells are interesting from other perspectives as well. The catalytic properties of the oxide surfaces, modified with the metal core, especially photocatalysis, are an important aspect.[11,12] The shells being porous at low thickness makes it possible for ions and molecules to diffuse through them. Apart from implications in catalysis, this also leads to changes in the dielectric constant, which results in changes in color. Modified properties such as electrical transport upon exposure to gases and ions are another important aspect. The shell being inert can be used to deliver metal colloids into reactive environments and can even be thought of as a mode to deliver drugs.[13] The possibility of removing the core by appropriate chemistry will leave behind a shell; the chemistry of such nanobubbles will be interesting.[14]

From all these perspectives, it is interesting and possibly desirable to make core−shell particles with oxide covers by simple and scalable procedures. In the following, we describe a method in four cases and provide detailed characterization of the materials. We shall touch upon one application we are pursuing currently, namely, optical limiting.

Experimental Section

$HAuCl_4 \cdot 3H_2O$ was purchased from CDH Chemicals. Titanium isopropoxide and zirconium(IV) propoxide were from Aldrich. All the solvents used in the synthesis were from local sources and were distilled prior to use. The chemicals were of the best purity available. The purity was not independently checked except for UV−vis absorption spectroscopy, wherever necessary.

In the procedure, a solution containing equimolar (19.9 mM) amounts of titanium isopropoxide (or zirconium(IV) propoxide) and acetylacetone in 2-propanol was prepared. A clear solution was formed upon mild sonication. Another solution of 8.80 mM $AgNO_3$ (or $HAuCl_4 \cdot 3H_2O$) and 13.88 M H_2O in DMF was prepared. A 40 mL sample of the first solution and 20 mL of the second solution were mixed and stirred for about 10 min. The mixture was transferred to a heating mantle and refluxed for 45 min. The solution became pink in the case of Au and green-black in the case of Ag. The color change was abrupt in the case of Au and more gradual in the case of Ag. Further refluxing of the solution resulted in the formation of a precipitate, which could be dispersed by sonication. The colloidal material was precipitated by the addition of toluene. The precipitate was washed repeatedly with toluene and redissolved in 2-propanol. The cleaning procedure is important to obtain well-defined absorption spectra and electrochemical properties discussed subsequently. Dry powders were not redispersible (thus, the 2-propanol dispersions contained traces of toluene). The solutions (mother liquor as well as redispersed particles) were stable for over two months. Ag particles were more dispersible than Au particles; the latter showed aggregation with passage of time. Dispersibility was better with $Ag@ZrO_2$ than $Ag@TiO_2$. Upon slow evaporation of the solvent, a gel was formed for $Au@TiO_2$; the critical gelation concentration varied with the thickness of the shell. In all cases, the shell thickness was varied by increasing the precursor concentration, keeping the reaction time constant (in most of the cases).

Initial transmission electron microscopy (TEM) measurements were performed with a Philips CM12 microscope working at 120 keV acceleration. Later measurements used a JEOL 300 keV high-resolution instrument (HRTEM). The sample solution was drop-casted onto carbon-coated copper grids. X-ray diffraction studies were carried out with a Shimadzu XD-D1 diffractometer with Cu Kα radiation (30 kV, 20 mA). The samples were spread onto antireflecting glass slides and were wetted with acetone to obtain a uniform film. Acetone was blown dry, and the slide was mounted onto the diffractometer. IR spectroscopic measurements were performed with a Bruker IFS 66v FT-IR spectrometer. All samples were prepared in the form of 1% (by weight) KBr pellets. UV−vis spectra were measured in a Varian Cary 5 UV−vis−near-IR spectrophotometer. X-ray photoelectron spectroscopic measurements were carried out with a VG ESCA LAB MkII instrument at the Notre Dame University, Notre Dame, IN, and Indian Institute of Science, Bangalore, using Mg Kα and Al Kα radiations, respectively. The measurements were done with 20 eV pass energy, and 10 scans were averaged. The binding energies were corrected with the C 1s peak at 285 eV binding energy as the samples exhibited mild charging. Thermal analyses were carried out on a NETZSCH STA 409 thermal analysis instrument. A heating rate of 10 deg/min was used for the measurements, and about 15 mg of the sample was used. Data in the range of 25−1400 °C were collected. The measurements were made in a nitrogen atmosphere. Cyclic voltammograms were obtained on an electrochemical analyzer (CH Instruments model 600A) in a standard three-electrode cell comprising a Pt disk (area 0.8 mm^2) as the working electrode, a platinum foil as the counter electrode, and Ag/AgCl as the reference electrode. Voltammetry was performed at a scan rate of 100 mV/s in a propanol/acetonitrile (1:1 v/v) mixture containing 0.1 M tetrabutylammonium hexafluorophosphate ($TBAPF_6$) as the supporting electrolyte. The precipitated core−shell particles were dispersed in 2-propanol by sonication. This process was repeated three times to remove DMF and impurities formed in the reaction. To the purified dispersion of core−shell particles in 2-propanol was added drop by drop with stirring an equal volume of a millimolar solution of stearic acid ($CH_3(CH_2)_{16}COOH$) to get monolayer protected particles. The solution was stirred for 30 min after addition. Optical limiting measurements were carried out at 532 nm in solution, using 7 ns laser pulses produced by a frequency-doubled Spectra Physics Nd:YAG laser (GCR-150). Solutions were prepared by dissolving the samples in a mixture of DMF and 2-propanol. Limiting data were extracted from open aperture *z*-scan experiments[15] where a 1 mm cuvette containing the sample was scanned through the focal plane of a lens that focuses the laser beam. The laser pulses were plane polarized with a Gaussian spatial profile.

Results and Discussion

Synthesis. Reaction of Ag^+ with DMF has been reported before.[5,16] Catalytic production of hydrogen from DMF/H_2O mixtures in the presence of a platinum catalyst was reported by Vaska et al.[17] Liz-Marzan and co-workers[5] concluded that the process involved the reaction $HCONMe_2 + 2Ag^+ + H_2O \rightarrow 2Ag^0 + Me_2NCOOH + 2H^+$, which has been supported by an increase in the conductivity of the solution. The carbamic acid thus formed easily decomposes to CO_2 and Me_2NH.[17] A similar reaction is expected to occur for gold, which in our case can be written as $3HCONMe_2 + 2AuCl_4^- + 3H_2O \rightarrow 2Au^0 + Me_2NCOOH + 6H^+ + 8Cl^-$; the presence of these ions in the medium was verified by separate experiments. To understand the reduction process clearly, the reaction mixture was analyzed by GC−MS (HP 5987). In all the measurements, the principal products detected were the starting materials. No bulk gas evolution was detected, and the pressure

(11) Kakuta, N.; Park, K. H.; Finlayson, M. F.; Veno, A.; Bard, A. J.; Campion, A.; Fox, M. A.; Webber, S. E.; White, J. M. *J. Phys. Chem.* **1985**, *89*, 3828.

(12) Nasr, C.; Chandini, H. S.; Kim, W. Y.; Schmehl, R. H.; Kamat, P. V. *J. Phys. Chem. B* **1997**, *101*, 7480.

(13) (a) Davis, S. S. *Trends. Biotechnol.* **1997**, *15*, 217. (b) Tomilson, S.; Taylor, P. W.; Luzio, J. P. *Biochemistry* **1989**, *28*, 1989.

(14) (a) The electrochemistry of nanoshells has been demonstrated already. See: Koktysh, D. S.; Liang, X.; Yun, B.-G.; Pastoriza-Santos, I.; Matts, R. L.; Giersig, M.; Serra-Rodriguez, C.; Liz-Marzan, L. M.; Kotov, N. A. *Adv. Funct. Mater.* **2002**, *12*, 255−265. (b) ZrO_2 shells have been prepared using a new kind of chemistry in which halocarbons are used to leach out metal cores: Nair, S. K.; Tom, R. T.; Suryanarayanan, V.; Pradeep, T. *J. Mater. Chem.* **2003**, *13*, 297−300.

(15) Sheik-Bahae, M.; Said, A. A.; Wei, T. M.; Hagan, D. J.; Van Stryland, E. W. *IEEE J. Quantum Electron.* **1990**, *26*, 760.

(16) Reaction with $AuCl_4^-$ has been reported recently. See: Pastoriza-Santos, I.; Liz-Marzan, L. M. *Langmuir* **2002**, *18*, 2888−2894.

(17) James, Y. Yu.; Serge Schreiner.; Vaska, L. *Inorg. Chim. Acta* **1990**, *70*, 145−147.

above the reaction vessel did not register any change; we conclude that no evolution of CO_2 occurred. The CO_2 formed, if any, may have dissolved in the solution or adsorbed on the oxide surfaces. To reduce the complexity of the system under investigation, separate GC−MS studies were done to understand the DMF-induced reduction process itself (without the oxide precursor). In these experiments, only DMF, water, and $AgNO_3$ were used as the starting materials, and we detected Me_2NH. No gas evolution was detected, even after the reaction was scaled up. The only appreciable change detected was the large increase in the conductivity of the solution as well as a decrease in the pH. For Au-based synthesis, the final pH was 3.5, while it was 2.5 for Ag. In view of all these experiments, we support the earlier conclusion that the reduction reaction proceeds through carbamic acid, although CO_2 by itself could not be detected. We are aware that the reduction process could follow two other pathways, namely, the carbon monoxide route and the formic acid route,[17] but both would give hydrogen as one of the products. It is unlikely that it was trapped completely in the condensed phase, favoring the carbamic acid route. The lifetime of carbamic acid appears to be too small to be detected by GC−MS. No other chemical species were detected even when the reaction products were analyzed as a function of time. The gas volume above the reaction vessel was also sampled during the course of the reaction, and no additional products were observed.

UV−Vis Absorption Spectroscopy. Formation of colloids was monitored by UV−vis absorption spectroscopy. The peak maximum corresponding to the plasmon excitation of gold typically occurs around 520 nm in organic solvents.[18] The peak red shifts as the gold cluster surface is covered with an oxide layer (Figure 1). There are two kinds of shifts, shifts upon encapsulation and shifts upon increasing the particle dimension. The shift in plasmon upon encapsulation is attributed to the dielectric constant of the surrounding matrix upon encapsulation. For noninteracting spheres, Mie's theory explains the absorption and scattering of essentially spherical particles.[19] This theory has been extended and modified to include several other systems such as nonspherical ones and coated spheres. If one takes only the dipole process into account, the classical plasmon frequency is proportional to $(Ne^2/Km\epsilon_0)^{1/2}$, where N is the free electron density, e is the electronic charge, m is the electron mass, K is the dielectric constant, and ϵ_0 is the permittivity of free space.[20] Simple dielectric theory has been used to explain the optical absorption spectra of silica-coated gold particles, but the onset of quantum size effects leads to deviations from bulk dielectric behavior. On silica encapsulation, the peak red shifts as predicted by Mie's theory.[7]

While the peak maximum shifts to the red, the shell also affects the width of the peak. An increase in shell thickness increases the peak width. In a classical sense, the width is related to the collision time, and an increase in width implies that the metal clusters are becoming more isolated with less and less electronic interactions between nearby units. This is expected as the oxide shell thickness increases. This behavior is also seen in the case of metal colloids protected with alkanethiolates[18b] as a function of increasing chain length. Thus, the increase in width is explained as due to the confinement of the free electrons within the metal core. However, this is true only in the case of smaller particles, where the particle dimension is much smaller than the wavelength of electrons (below 25 nm, for gold particles).[19] The increase in width with chain length is better manifested in the condensed phase when particles are in close contact and not when the particles are in solution.

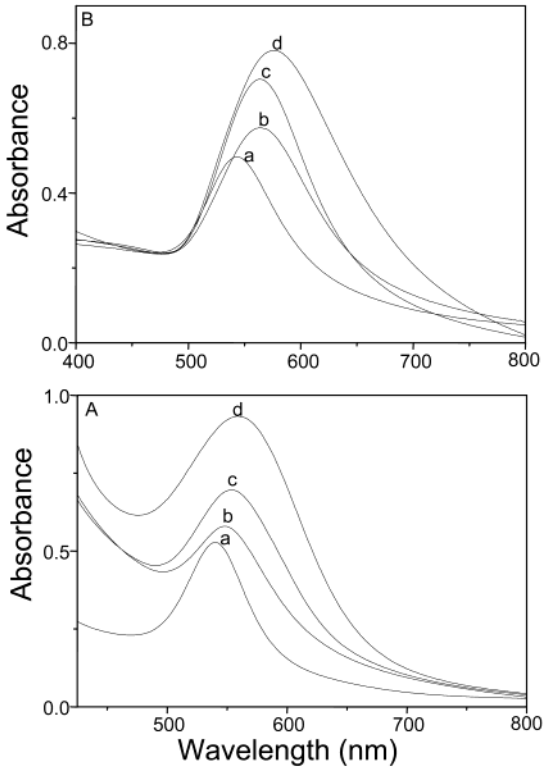

Figure 1. (A) UV−vis absorption spectra of TiO_2-covered Au nanoparticles as a function of Au^{3+} concentration in the reaction mixture. The peak maxima are 540 (a), 548 (b), 554 (c), and 560 (d) nm for Au^{3+} concentrations of 1.3, 2.6, 3.9, and 5.3 mM, respectively. Note the increase in the width of the peaks. (B) UV−vis absorption spectra of ZrO_2-covered Au particles. Curves a and c correspond to ZrO_2 concentrations of 19.9 and 39.8 mM, respectively (keeping the Au^{3+} concentration at 5.4 mM). The peak maximum shifts from 543 to 564 nm. The same effect occurs in increasing the reaction time from 45 to 90 min at 5.4 mM concentration (a and b), respectively, and at 39.8 mM concentration (c and d), respectively.

For larger particles, such as the ones prepared here, the plasmon peak red shifts and increases in width with an increase in particle dimension.[19] The increase in width, however, is attributed to inhomogeneous polarization of the particle in the electromagnetic field and associated retardation as well as multipole excitation effects. This is referred to as the extrinsic size effect. As can be seen in Figure 1A, the curves exhibit much change in width. We attribute these changes to an increase in the particle dimension in the extrinsic size range, as demonstrated before.[19] Note that the only parameter changed in these samples is the Au^{3+} concentration, which changes the average particle size. It is very possible that the shape of the particles affects the plasmon band position, since it is clear in TEM that many of the particles are elongated (see below). However, no drastic shape changes were observed in the particle morphology in TEM studies of different samples with varying Au^{3+} concentration.

(18) (a) Brust, M.; Walker, M.; Bethell, D.; Schiffrin, D. J.; Whyman, R. *J. Chem. Soc., Chem. Commun.* **1994**, 801−802. (b) Sandhyarani, N.; Resmi, M. R.; Unnikrishnan, R.; Ma, S.; Vidyasagar, K.; Antony, M. P.; Panneer Selvam, G.; Visalakshi, V.; Chandrakumar, N.; Pandian, K.; Tao, Y.-T.; Pradeep, T. *Chem. Mater.* **2000**, *12*, 104−113.

(19) Link, S.; El-Sayed, M. A. *J. Phys. Chem. B* **1999**, *103*, 8410−8426.

(20) Heath, J. R.; Knobler, C. M.; Leff, D. V. *J. Phys. Chem. B* **1997**, *101*, 189−197.

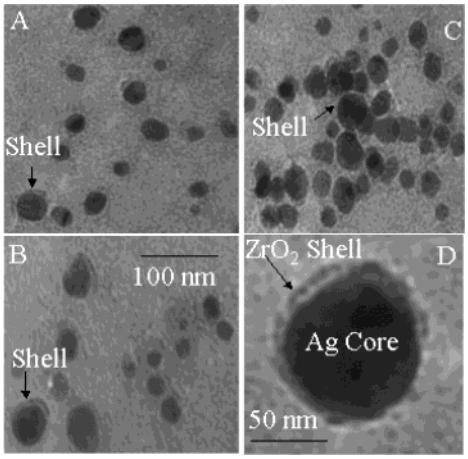

Figure 2. Transmission electron micrographs of ZrO_2-covered Ag particles. Photographs A−C are collections of particles from various portions of the grid; the images are of the same magnification. Photograph D is an expanded view of one particle. The image has not been manipulated digitally. The shell is marked.

An increase in the oxide thickness can also be used to shift the peak maximum as well as width.[21] This is demonstrated in the absorption spectrum of Au@ZrO_2 (Figure 1B), where a red shift is brought about by both increasing the concentration of the oxide precursor and increasing the hydrolysis time, keeping all other parameters the same. For curves a and c, the concentration of zirconium(IV) propoxide varied from 19.9 to 39.8 mM and the peak shifted from 543 to 564 nm (keeping a reaction time of 45 min). A similar effect is brought about by varying the reaction time from 45 to 90 min, keeping the concentration constant. Graphs a and b correspond to reaction times of 45 and 90 min at a ZrO_2 concentration of 19.9 mM, while graphs c and d correspond to the same times at 39.8 mM. In all these cases, the Au^{3+} concentration was 5.4 mM. An increase in the reaction time allows hydrolysis to occur to a greater extent over the cluster. As a result of the increase in shell thickness, the peak width increases, and it is evident in these spectra. An increase in the reaction time does not change the core size or shape distribution as revealed by TEM.

The absorption spectra of the corresponding Ag particles show a similar effect. As the concentration of zirconium(IV) propoxide increases from 19.9 to 79.6 mM, the absorption maximum increases from 409 to 425 nm.

Electron Microscopy. Initial measurements were done with a CM12 instrument, which did not reveal the shell clearly. Cores were clearly observable, but there was no sharp contrast for the shell. Subsequent images were collected with a JEOL 300 keV HRTEM instrument, and several images are shown in Figure 2.

The figure shows a collection of ZrO_2-covered silver particles with an absorption maximum of 425 nm. The particle size is 45 ± 15 nm along one axis, and a range of particle morphologies are seen. Although most of the particles seen in this image are spherical or oval, faceted structures were also observed. The shell is evident on each particle. The shell of ZrO_2 was more distinct than that of TiO_2, and more TEM studies were done with this material. A closer look at each of these particles reveals that the shells are completely covering the particles (Figure 2D). There appears some nonuniformity in the shell thickness, yet the coverage is complete. The typical shell thickness is in the range of 2−3 nm. No diffraction was seen from the shells, but the cluster cores manifested bulk fcc patterns; a [111] zone axis was observed. Although different core sizes are seen, by controlling chemical conditions, it is possible to obtain smaller core sizes. Microscopy did not reveal free particles of metals or oxides. The presence of completely covering shells is confirmed with reactivity studies as well (see below). The core size or distribution did not change by increasing the reaction time or increasing the concentration of the oxide precursor.

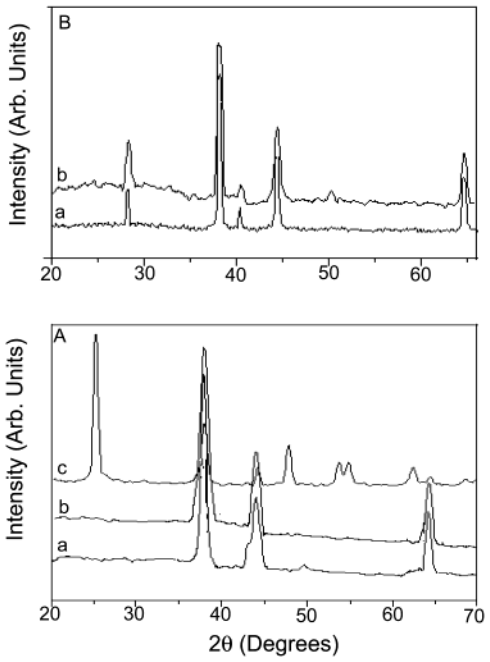

Figure 3. (A) XRD patterns of Au@TiO_2 core−shell particles showing an absorption maximum at 554 nm: (a) sample dried at room temperature, (b) sample after heating to 200 °C, and (c) sample after heating to 650 °C. Note the emergence of peaks at 25.3 in (c) due to TiO_2 (anatase). All the other new peaks in (c) are also due to anatase. (B) XRD patterns of Au@ZrO_2 particles. (a) and (b) correspond to the same preparative conditions as (b) and (d) in Figure 1B.

X-ray Diffraction. X-ray diffractograms of the materials were studied as a function of shell thickness (Figure 3). The core manifests peaks due to (111), (200), and (220) reflections corresponding to bulk fcc Au in all the samples. The peak widths correspond to an average particle diameter of 50 nm as derived from the Scherrer formula (for Au@TiO_2). For particles of different absorption maxima, the Au reflections do not change significantly, and it appears that XRD is not sensitive to the changes in particle dimension in this range (30−50 nm). The shell appears to be amorphous at room temperature as no peaks due to it appear. Upon heating the sample to 200 °C for 5 h, the peaks remain the same (trace b); reflections due to TiO_2 are still not present. However, upon heating the sample to 650 °C, a pattern resembling a mixture of anatase and gold appears (trace c; note the peak at 25.3°). The sample appears black as a result of finely divided metal. We believe that the metal came out of the shell after melting. The material could not be examined by TEM. The amorphous nature of the shell in the parent material is in accordance with the TEM results.

For Au@ZrO_2, an unidentified peak shows up at 27° in the as-prepared material. The intensity of this peak increases with the shell thickness, as expected. In Figure 3B, samples a and b correspond to samples b and d in Figure 1B. These correspond to zirconium(IV) propoxide concentrations of 19.9 and 39.8 mM for a reaction time of

(21) Alejandro-Arellano, M.; Ung, T.; Blanco, A.; Mulvaney, P.; Liz-Marzan, L. M. *Pure Appl. Chem.* **2000**, *72*, 257−267.

90 min. As mentioned before, this change in conditions would have resulted in an increased thickness corresponding to longer hydrolysis time. Note that the relative intensity of the peak at 27° (compared to the gold peaks) has increased. The peaks due to monoclinic zirconia appear in samples heated to 250 °C. The corresponding Ag samples present almost identical behavior; the major reflections of the monoclinic phase at 28° (−111) and 31° (111) appear in all the Ag samples.

Infrared Spectroscopy. To characterize the molecular nature of the material, infrared spectra of the samples were taken. All the spectra were measured in KBr matrixes. The air-dried sample of $Au@TiO_2$ shows characteristic peaks due to DMF. The peaks observed at 2920, 1676, 1260, and 1020 cm^{-1} are due to C(O)−H, C═O,C-(O)−N, and N−CH_3 stretching modes, respectively, of DMF, as reported in the literature.[22] The spectrum also shows characteristic broad hydroxyl stretches corresponding to the surface −OH groups. This peak remains even after the sample is heated to 100 °C. However, upon heating to 200 °C, a characteristic broad peak at 500 cm^{-1} appears. There are specific features in them, such as the one at 531 cm^{-1} attributed to Ti−O−Ti stretching.[23] Further heating to 650 °C results in the loss of the entire infrared features corresponding to the melting of the core and formation of a conducting sample. The material at this stage is a conducting black solid (IR spectra are presented in the Supporting Information).

The infrared spectrum confirms the molecular nature of the $Au@ZrO_2$ sample. The IR spectrum of zirconia is strongly sensitive to the solid-state structure. In all the phases, the spectrum has features below 725 cm^{-1}; the distinct features depend on the structure. In all the samples, a feature at 530 cm^{-1} appears attributed to the F_{1u} mode in the cubic phase, corresponding to the Zr−O−Zr stretch.[24] Degeneracy is lifted and additional modes are manifested in the tetragonal and monoclinic phases. The spectrum shows features corresponding to DMF as mentioned above. Two distinct features around 725 and 525 cm^{-1} appear, assigned to the Zr−O−Zr stretch. The material is a hydrated zirconia phase, with chemisorbed solvent molecules. Upon removing the metal core, well-developed IR features of zirconia are observed, similar to the cubic phase.[14b]

The IR spectra did not vary with variation in the plasmon feature. The presence of a solvated oxide cover is evident in the IR spectra. Thermal treatment removes the solvent, and features due to the oxides appear. Metalization of the oxide can occur upon heating at 650 °C.

Electrochemical Properties. For CV measurements, 10 mL of the colloidal dispersion in 2-propanol was mixed with 10 mL of 0.2 M $TBAPF_6$ in CH_3CN. The resultant solution was degassed by purging with nitrogen gas for 5 min, and voltammetry was performed. By dipping the Pt electrode into the dispersion, colloidal particles become adsorbed on the electrode surface. In Figure 4A, the Ag_m/Ag_m^+ couple is observed[25] at $E_{p1/2} = 250$ mV, which was confirmed by various experiments. The electron transport has to be sensitive to the ZrO_2 matrix. When we adsorb a long-chain fatty acid such as stearic acid on the ZrO_2 matrix, the cover can inhibit electron transport. In accordance with this, we see that the peak current is diminished by increasing the stearic acid concentration (a−f). Quenching of the peak current linearly with stearate adsorption proves that the zirconia shell is covering the Ag nanoparticle. A change in the peak potential is interpreted as due to variation in electron-transport mechanisms as a result of adsorption. The same kind of study was performed with $Au@ZrO_2$. The peak intensity of Au_n/Au_n^+ ($E_{p1/2} = 320$ mV)[26] was also quenched by increasing the stearic acid concentration as shown in Figure 4B. The next set of experiments were done with titania-protected clusters under identical conditions. Quenching of Ag_m/Ag_m^+ and Au_n/Au_n^+ peaks by increasing the stearic acid concentration is presented in parts A and B, respectively, of Figure 5.

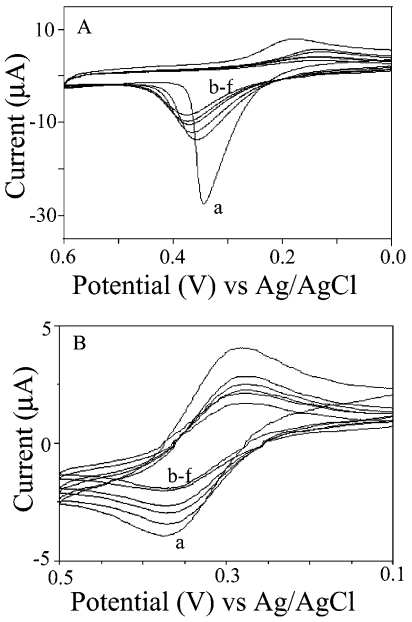

Figure 4. (A) Cyclic voltammograms of ZrO_2-covered Ag nanoparticles with varying amounts of stearic acid absorbed. Cyclic voltammogram a is for the parent $Ag@ZrO_2$ particles; cyclic voltammograms b−f are for the stearic acid adsorbed particles containing 4, 6, 8, 10, and 12 mM stearic acid, respectively. The concentration of the core−shell particles is the same in all the cases. (B) Cyclic voltammogram of ZrO_2-covered Au nanoparticles with varying amounts of stearic acid absorbed. Cyclic voltammogram a is for the parent $Au@ZrO_2$ particles; cyclic voltammograms b−f are for the stearic acid adsorbed particles containing 4, 6, 8, 10, and 12 mM stearic acid, respectively. The concentration of the core−shell particles is the same in all the cases.

As carboxylic acids can bind silver directly, the effect of stearic acid adsorption on bare silver nanoclusers was investigated. This was to make sure that the adsorption was occurring on the oxide shell of the core−shell particles and not on the metal core. The citrate-capped silver nanoparticles change color from yellow to green after the adsorption of stearic acid, and in the case of $Ag@ZrO_2$ core−shell particles, no color change was observed. The UV−vis absorption spectrum of citrate-capped Ag nanoparticles shows a drastic change, while the spectrum of $Ag@ZrO_2$ exhibits only a slight (<5 nm) red shift in λ_{max}, as expected. This study also shows that the metal surface is covered by a complete oxide shell. The electrochemical behavior for all the systems is similar, indicating that the shell structure is similar in all the systems.

(22) Silverstein, R. M.; Webster, F. X. *Spectrometric Identification of Organic Compounds*; John Wiley and Sons: New York, 1998.

(23) (a) Ross, S. D. *Inorganic Infrared and Raman Spectra*; McGraw-Hill: London, 1972. (b) Nakamoto, K. *IR Spectra of Inorganic and Coordination Compounds*; John Wiley and Sons: New York, 1970.

(24) (a) Enrique, F. L.; Vicente, S. E.; Marta, P.; Maria, M. C.; Guido, B. *J. Mater. Chem.* **2001**, *11*, 1891−1897.

(25) Aslam, M.; Mulla, I. S.; Vijayamohanan, K. *Langmuir* **2001**, *17*, 7487.

(26) Bandyopadhyay, K.; Sainkar, S. R.; Vijayamohanan, K. *J. Am. Ceram. Soc.* **1999**, *82*, 222−224.

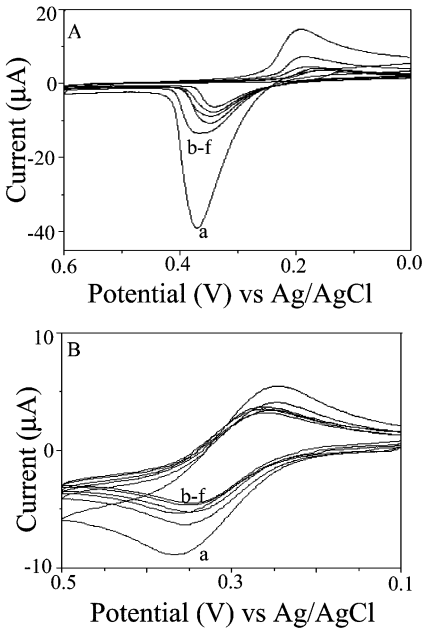

Figure 5. (A) Cyclic voltammograms of TiO_2-covered Ag nanoparticles with varying amounts of stearic acid absorbed. Cyclic voltammogram a is for the parent Ag@TiO_2 particles; cyclic voltammograms b−f are the stearic acid adsorbed particles containing 4, 6, 8, 10, and 12 mM stearic acid, respectively. The concentration of the core−shell particles is the same in all the cases. (B) Cyclic voltammogram of TiO_2-covered Au nanoparticles with varying amounts of stearic acid absorbed. Cyclic voltammogram a is for the parent Au@TiO_2 particles; cyclic voltammograms b−f are the stearic acid adsorbed particles containing 4, 6, 8, 10, and 12 mM stearic acid, respectively. The concentration of the core−shell particles is the same in all the cases.

We have studied the adsorption chemistry with another system. *cis*-Dithiocyanatobis(2,2′-bipyridyl-4,4′-dicarboxylic acid)ruthenium(II) dye was adsorbed on Au@TiO_2 particles. This molecule has been used for dye-sensitized photovoltaic cell applications[27] and is known to exhibit specific binding on nano-TiO_2. The peak current in CV was significantly reduced as a result of adsorption. This shows that ion transport possible in the original particles is hindered by adsorption. Quenching of the peak current of the quasi-reversible Ag_m/Ag_m^+ couple as well as the quasi-reversible Au_n/Au_n^+ couple upon stearic acid adsorption confirms the complete nanoporous oxide shell structure around Ag and Au metal clusters. Ion-transport characteristics can be used to study the porosity of the shell, and this aspect will be published separately.[28]

Additional Characterization. Valence states of various elements were investigated by X-ray photoelectron spectroscopy. All the materials contain the expected elements. The intensities of the Au 4f and Ag 3d photoelectrons were poor due to the shell contributing to the intensity loss. The core was found to be metallic. The Ti and Zr were in their tetravalent states as the Ti $2p_{3/2}$ and Zr $3d_{5/2}$ binding energies were 458.0 and 182.0 eV, respectively.[29] O 1s in all cases was seen at 532.0 eV binding energy. In the case of Au@ZrO_2, the thickness of the shell was low enough to see Au 4f clearly. Au $4f_{7/2}$ was observed at 84.0 eV, characteristic of metallic Au. Ag $3d_{5/2}$ was observed at 368.0 eV, corresponding to metallic Ag. Slight charging (on the order of 1.5 eV) was observed for the powder samples, as expected for an insulating cover, and the binding energies were corrected with the C 1s contaminant peak at 285 eV binding energy. Significant carbon contamination was observed in the as-prepared sample in accordance with the infrared spectrum and thermogravimetry (TG) data. Nitrogen was not seen, possibly due to desorption of adsorbed DMF under vacuum.

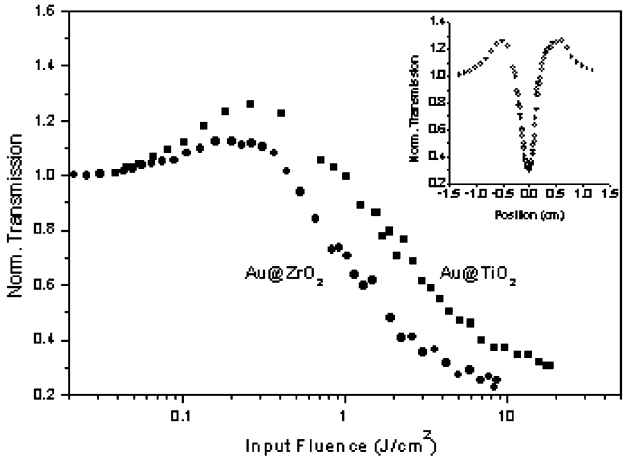

Figure 6. Optical limiting exhibited by the samples at 532 nm. The linear transmission is 0.64 for the Au@ZrO_2 sample and 0.49 for the Au@TiO_2 sample (the absorption peaks are at 564 and 554 nm, respectively). The inset shows the *z*-scan curve obtained for Au@TiO_2.

TG data of Au@TiO_2 samples were measured up to 1400 °C. The samples essentially present a two-step mass loss, one in the range of 100−200 °C, corresponding to the desorption of solvents as manifested in IR. The second loss, corresponding to less than 5%, occurs in the range of 600−800 °C. This is attributed to dehydration of surface hydroxyl groups. Hydroxyl groups are present in the IR spectrum for the sample heated to 250 °C. As the gold concentration increases (corresponding to longer wavelength absorption), the samples show less and less mass loss, suggesting that gold is retained in the residue. As the titanium precursor concentration was constant in all the preparations, the percentage of TiO_2 precursor species is larger when the amount of Au is lower. These samples contain a larger percentage of adsorbed water and solvents, contributing to the larger mass loss. As the oxide cover is solvated with unclear stoichiometry, we did not attempt to analyze the data further. In the case of ZrO_2, TG shows more desorption structures. However, an increase in the shell thickness is manifested in the weight loss.

Optical Limiting Studies. Our previous studies had shown that ligand-protected gold and silver nanoclusters and their alloys are good optical limiters for nanosecond and picosecond laser pulses.[9,30] To investigate the nonlinear behavior of the present samples, we measured the transmission of 7 ns laser pulses with input fluences ranging from 0.02 to 20 J/cm^2 (equivalent to an increase of the peak intensity from 2.8 MW/cm^2 to 2.8 GW/cm^2) through the sample solutions. Results obtained for the Au colloids are shown in Figure 6, and the inset shows the *z*-scan curve obtained for Au@TiO_2. Transmission values are normalized to the value obtained for the lowest input fluence, which is taken as unity. The figure shows an increase in transmission around 0.2 J/cm^2, followed by a strong reduction in the transmission at higher fluences.

(27) Kalyanasundaram, K.; Gratzel, M. In *Optoelectronic Properties of Inorganic Solids*; Roundhill, D. M., Fackler, J. P., Jr., Eds.; Plenum Press: New York, 1999; pp 169−194.

(28) Suryanarayanan, V.; Nair, S. K.; Tom, R. T.; Pradeep, T. To be published.

(29) Briggs, D.; Seah, M. P. *Practical Surface Analysis*; John Wiley & Sons: New York, 1983; p 493.

(30) Philip, R.; Mujumdar, S.; Ramachandran, H.; Kumar, G. R.; Sandhyarani, N.; Pradeep, T. *Nonlinear Opt.* **2001**, *27*, 357.

For the Au@ZrO_2 nanoparticle, the onset of limiting is around 0.5 J/cm^2 while the normalized transmission drops to 0.3 at 4 J/cm^2, and these values indicate a better limiting efficiency than that of single-walled carbon nanotube suspensions[31] and metal−dendrimer nanocomposites.[32]

To explain the optical limiting activity of metal nanoparticles, an RSA (reverse saturable absorption) type mechanism and nonlinear scattering have been recently suggested. For example, the optical limiting response of silver bromide nanoparticles in nanosols[33] and that of suspended silver-containing nanoparticles[34] have been attributed to the formation of a photogenerated, strongly absorptive intermediate species. Similarly Kamat and co-workers[35] assigned the strong, broad-band transient absorption observed in colloidal silver particles of 40−60 nm diameter to a transient state that is generated in a photoinduced intraparticle charge separation process. On the other hand, from comparative studies in gold clusters of 5 and 30 nm average diameters, Mostafavi and co-workers[36] have explained the nanosecond limiting shown by these samples in the framework of nonlinear scattering. We believe that the presently observed optical limiting can be a cumulative outcome of these phenomena.

A significant point about the oxide-protected colloids is that their laser damage thresholds are definitely higher than those of the ligand-protected clusters, and this is very important from the device point of view. We have obtained similar results in the Ag colloids as well. More experiments are being conducted in this direction, and will form the subject matter of a future publication.

Summary and Conclusions

Au and Ag core−shell particles with TiO_2 and ZrO_2 covers of varying thickness were made in a one-step synthetic route. The process could be adapted for the synthesis of bulk core−shell materials. The product can be washed and redispersed. The solution is stable for extended periods. The cover is amorphous with a high content of the solvent, but upon heat treatment becomes a crystalline oxide. Absorption spectroscopy, electron microscopy, X-ray diffraction, infrared spectroscopy, cyclic voltammetry, XPS, and TG were used to reveal various properties of the material. Nonlinear optical measurements indicate that these materials are strong optical limiters with a high laser damage threshold. Selective functionalization of the oxide shells with organic molecules to improve solubility is being pursued currently.

Acknowledgment. T.P. acknowledges financial support from the Government of India, Ministry of Information Technology, and Space Technology Cell of the Indian Institute of Technology Madras. He thanks Prof. M. S. Hegde and Dr. Bindhu Varughese for the XPS measurements. Dr. Ram Devanathan and Ms. Kanchanamala are thanked for assistance with the TEM. Dr. Md. K. Nazeeruddin, EPFL, Lausanne, is thanked for a gift of the *cis*-dithiocyanatobis(2,2′-bipyridyl-4,4′-dicarboxylic acid)-ruthenium(II) dye sample. Mr. Hami Òz is thanked for the GC−MS measurements.

Supporting Information Available: Infrared spectra of Au@TiO_2 and Au@ZrO_2 particles. This material is available free of charge via the Internet at http://pubs.acs.org.

LA0266435

(31) Mishra, S. R.; Rawat, H. S.; Mehendale, S. C., Rustagi, K. C.; Sood, A. K.; Bandopadhyay, R.; Govindaraj, A.; Rao, C. N. R. *Chem. Phys. Lett.* **2000**, *317*, 510.

(32) Ispasoiu, R. G.; Balogh, L.; Varnavski, O. P.; Tomalia, D. A.; Goodson, T. *J. Am. Chem. Soc.* **2000**, *122*, 11005−11006.

(33) Sahyun, M. R. V.; Hill, S. E.; Serpone, N.; Danesh, R.; Sharma, D. K. *J. Appl. Phys.* **1996**, *79*, 8030.

(34) Sun, Y.-P.; Riggs, J. E. *Int. Rev. Phys. Chem.* **1999**, *18*, 43. Sun, Y.-P.; Riggs, J. E.; Rollins, H. W.; Guduru, R. *J. Phys. Chem. B* **1999,** *103*, 77.

(35) Kamat, P. V.; Flumiani, M.; Hartland, G. V. *J. Phys. Chem. B* **1998**, *102*, 3123.

(36) Francois, L.; Mostafavi, M.; Belloni, J.; Delouis, J.-F.; Delaire, J.; Feneyrou, P. *J. Phys. Chem. B* **2000**, *104*, 6133.